Proceedings of ASME FEDSM'01
2001 ASME Fluids Engineering Division Summer Meeting
New Orleans, Louisiana, May 29- June 1, 2001

FEDSM2001-18111

EXPERIMENTAL CLASSIFICATION OF TURBULENCE IN AN OSCILLATORY CHANNEL FLOW WITH TRANSPIRING WALLS

J. Majdalani[1]
Department of Mechanical Engineering
Marquette University, Milwaukee, WI 53233
Email: maji@marquette.edu

J. Barron and W. K. Van Moorhem
Mechanical Engineering Department
University of Utah, Salt Lake City, UT 84112

In this work, the onset of turbulence inside a rectangular chamber is investigated, with and without side-wall injection, in the presence of an oscillatory pressure gradient. Two techniques are used to define the transition from laminar to turbulent regimes: statistical analysis and flow visualization. Calibrated hot film anemometry and a computer data acquisition system are used to record and analyze acoustical flow data. Four classifications of flow regimes are reported: (a) laminar, (b) distorted laminar, (3) weakly turbulent, and (4) conditionally turbulent. Despite numerous attempts to promote turbulence, a fully turbulent flow does not develop at any of the driving frequencies tested. Based on statistical measurements, a periodic drop in standard deviation always occurs, indicating relaminarization within each cycle. Transition between flow regimes is assessed from the standard deviation of velocity data correlated as a function of the acoustic Reynolds number. Under predominantly laminar conditions, the standard deviation is found to vary approximately with the square of the acoustic Reynolds number. Under turbulent conditions, the standard deviation becomes almost directly proportional to acoustic Reynolds number. Transition in oscillatory flow with side-wall injection is found to be reproducible at the same critical value of the acoustic Reynolds number for $\mathrm{Re}_A = 200$.

1 INTRODUCTION

IN a solid rocket motor, it is both difficult and expensive to investigate the dynamic gas behavior associated with unsteady propellant burning. In fact, the presence of acoustic oscillations can affect the burning rate of known propellants, leading sometimes to serious combustion instabilities. In the current study, a simulation facility was constructed that employs solid carbon dioxide (dry ice) to simulate the response of a solid propellant. The use of dry ice makes it possible to mimic the surface gas addition that takes place inside rocket motors by isolating the fluid mechanical aspects from combustion elements. The current research includes modifying an existing simulation facility to implement new techniques and improve several experimental deficiencies reported previously. The work involves quantifying the occurrence of acoustically introduced turbulence and investigating flow phenomena that may exacerbate possible acoustic instabilities.

The mechanisms that trigger turbulence in steady flows are reasonably well understood. The main criterion for predicting turbulent regimes is based on the Reynolds number. Transition Reynolds numbers based on proper characteristic dimensions are well defined in a number of geometric configurations. Despite the considerable efforts devoted to turbulence, the issue of predicting turbulence in unsteady periodic flows remains, however, an open-ended question. In the spirit of improving our understanding of unsteady periodic flows, the current study has been undertaken. Our focus has been on assessing the criteria that may lead to turbulence for an oscillatory flow bounded by either hard or transpiring surfaces.

A variety of problems involving turbulent oscillatory flows are frequently encountered in the applied fields of acoustics and fluid mechanics. As previously mentioned in passing, one emerging topic is closely tied to combustion instability in solid rocket motors. In the rocket combustion instability community, it has become

[1] To whom correspondence should be addressed.

accepted that an acoustic boundary layer or 'Stokes layer' can stem from the oscillatory wave motion over a solid boundary. In fact, the instability of such oscillatory layers has been examined by several researchers in both circular-port and rectangular channels [1-10]. However, most previous experiments have been limited to the study of transitional Stokes layer behavior over nontranspiring surfaces. At present, we hope to extend those studies by incorporating the effects of gas addition at the walls.

2 BASIC IDEAS

For nonporous solid boundaries, the thickness of the oscillatory Stokes layer, δ, is found to be of the order of $\sqrt{2\nu/\omega}$ (where ν and ω are the kinematic viscosity and circular frequency). Under such physical settings, early investigators have noted that the onset of turbulence is governed by the Reynolds number based on the thickness of the boundary layer, $\mathrm{Re}_\delta = \delta U_0/\nu$. This similarity parameter has also been termed 'the acoustic Reynolds number' when written in the form

$$\mathrm{Re}_\mathrm{A} = \sqrt{\pi}\,\mathrm{Re}_\delta = U_0/\sqrt{f\nu}\,. \qquad (1)$$

In Eq. (1), U_0 is the amplitude of the oscillatory axial velocity component and $f = (2\pi\omega)$ is the frequency of oscillations.

Both experimental and theoretical analyses rise to a new level of difficulty when the flow boundaries are made porous. This becomes necessary when analyzing the burning response of propellants modeled as transpiring surfaces. Imposition of a normal influx along the porous walls introduces an additional complexity that must be dealt with. In fact, the incoming mean flow interaction with the internal acoustics can alter the flow considerably. From a physical standpoint, all parameters needed to characterize periodic flows remain valid here. The additional parameter of importance is the injection speed at the wall. On that account, the problem of predicting turbulence is expected to depend on the injection Reynolds number (based on the Stokes layer thickness and the injection velocity of the fluid). Investigations that correlate the turbulent character to the injection Reynolds number are hence necessary to help establish a clearer assessment of the flow stability criteria.

At the time of this writing, the oscillatory flow bounded by transpiring walls has been achieved experimentally by Traineau et al. [11], Ma et al. [12, 13], Huesmann and Eckert [14], and Dunlap et al.[15] Whereas Traineau and Ma have selected rectangular port chambers, Huesmann and Dunlap have employed circular-port tubes. Except for Ma's experiment, a pressurized gas injection was accomplished by forcing either air or nitrogen through sintered copper, aluminum or bronze plates. In all three experiments, the use of finely porous metal sheets was used to ensure the uniformity and homogeneity of mass addition.

In the current study, a different experimental technique is used to produce the desired injection. In fact, the sublimation of solid CO_2 is chosen over previously used simulation techniques for several reasons. Although weaker, the dynamic behavior of solid CO_2 is analogous to the behavior of an actual propellant. In a rocket motor, increasing the pressure results in an increase in propellant burn rate and, consequently, in the incoming mass flux. Similarly, an increase in the pressure over the solid CO_2 results in an increase in the sublimation rate and therefore mass flow from the surface. This increase is due to the drop in heat of sublimation with increasing pressure. Rather than using naturally transpiring surfaces, most cold flow facilities have simulated the combustion process by injecting gas through a porous wall. Under such circumstances, the pores must be choked to prevent acoustic energy from being lost into the walls. An increase in pressure above the porous walls results in either (a) unchoking of the pores and mass flow reduction or (b) a constant mass flow rate if the pores remain choked. These mechanisms may fail to capture some of the features associated with propellant burning. An even more serious problem is the possibility that the injection itself causes turbulence. The use of solid CO_2 eliminates the question of choking or unchoking at the pores and makes it ideally suited for simulating the behavior of a solid rocket motor propellant.

In addition to the novelty in effecting the gas evaporation from the walls, another advantage of this study is the careful selection of a Scotch-yoke wave generator that can produce purer harmonic waves than the rotary butterfly or slider-crank mechanisms used previously. Furthermore, unlike most previous experiments, the main focus of this experiment will be to characterize the flow regimes that arise prior to and during transition to turbulence.

3 EXPERIMENTAL APPARATUS

The Solid Carbon Dioxide Simulation Facility is a cold flow (nonreactive) facility. The use of solid carbon dioxide (CO_2 or dry ice) as the simulated propellant makes it possible to focus on the fluid mechanical aspects of the acoustic instability problem by separating the fluid mechanics from the combustion dynamics at the propellant surface. The Solid Propellant Rocket Motor Simulation Facility used in these experiments is shown in Fig. 1. The flow chamber has a square cross section with an inside dimension of 7.62 by 7.62 centimeters. The flow chamber consists of eight interchangeable sections, a

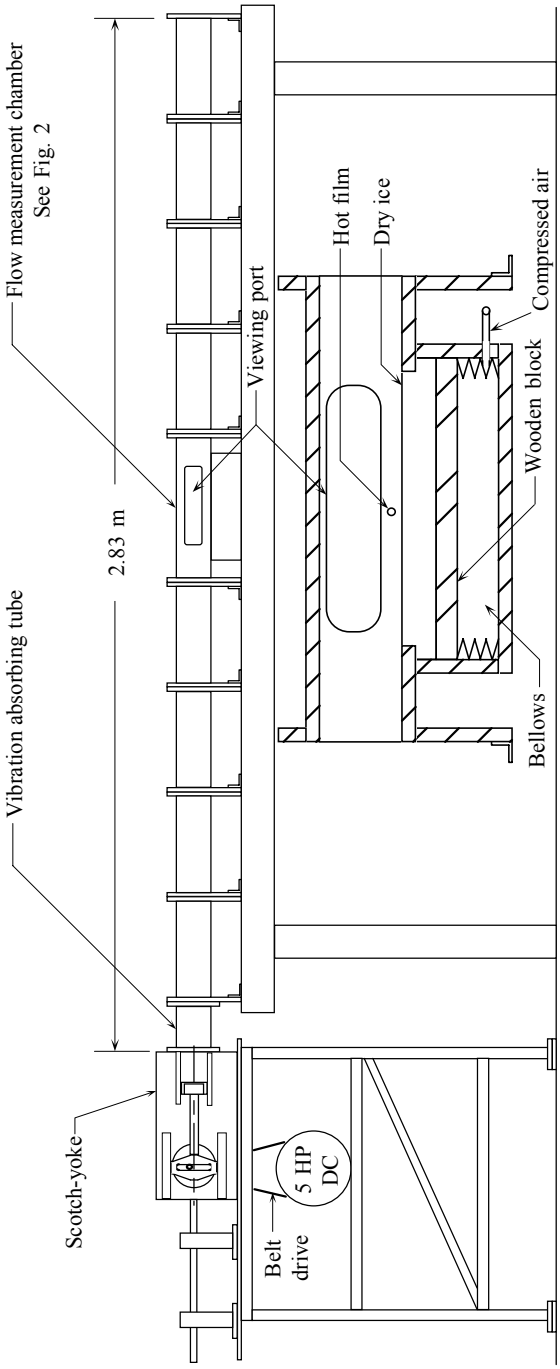

Fig. 1 Experimental apparatus. The inset shows a section view of the principal test chamber.

test section used for flow measurement, and a vibration isolating tube. The entire flow chamber is bolted to a heavy granite table to minimize vibration. The interchangeable sections make it possible to vary the test section location, chamber length and system resonant frequency. For these experiments, the length is held constant at 2.83 meters corresponding to a resonant frequency of 49 Hz at a temperature of 27 ^{o}C.

For all experiments, the chamber is initially purged with room temperature CO_2 gas to remove the air. The CO_2 gas enters at one end of the flow chamber and exits the chamber at the opposite end through a small orifice. The orifice is closed with a valve prior to operating the wave generator.

The principal part of the flow chamber is a 43.2 cm long test section (see Fig. 2). The test section is placed near the center of the chamber where the acoustic velocity antinode (maximum velocity) occurs and a pressure node (pressure minimum) occurs for a standing wave. This setup minimizes any pressure type of coupling in the dry ice sublimation. The inset in Fig. 1 shows a section view of the test section. Solid carbon dioxide is used in the test section to simulate solid propellant rocket motor characteristics. As explained above, the sublimation of solid CO_2 into gaseous carbon dioxide simulates the burning of the propellant. The solid CO_2 employed in this experiment is a commercial dry ice block approximately 30 cm long, 5 cm deep, and 7.62 cm in width. Thus it can be seated snugly at the bottom of the test section. The dry ice rests on a wooden block and a bellows is used to maintain the top of the dry ice at the same level as the bottom of the test section. The bellows pushes the dry ice with a constant supply air pressure of 3 psig. The bellows supply pressure is sufficiently large to eliminate significant vibration of the dry ice block due to acoustic pressure oscillations above the dry ice surface. The dry ice can be replaced with a fitted aluminum plate that makes the investigation of the flow field without side-wall injection possible. As shown in Fig. 2, glass view ports are located on either side of the test section to facilitate visual flow monitoring. The velocity of the gas near the surface of the dry ice can be measured by hot film anemometry. A hot film anemometer is mounted in the test section in order to measure local velocities. The hot film probe is centered above the dry ice and is located approximately 0.8 cm above the surface of the dry ice. The hot film probe is mounted perpendicularly to the dry ice surface.

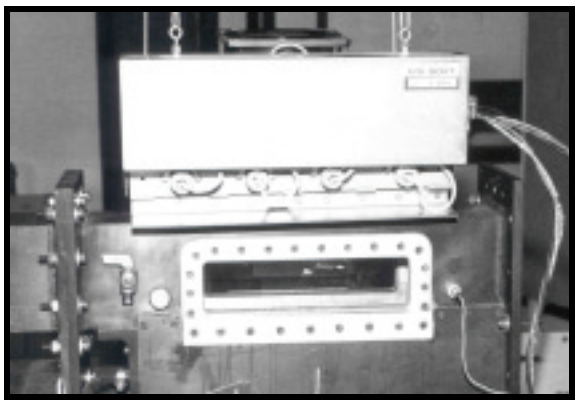

Fig. 2 Flow measurement chamber.

Pressure oscillations in the flow chamber can also be measured. A pressure transducer can be mounted at various locations in the chamber to record the pressure oscillations. For these experiments the pressure transducer was located at the end of the flow chamber counter-facing the wave generator where maximum pressure is observed.

The sublimation of solid CO_2 was chosen over previously used simulation techniques for reasons stated earlier. Several modifications were implemented as improvements to the experiments done by others. For example, an experimental difficulty in Ma's [12, 13] experiments was that a slider-crank mechanism (with a crankshaft, connecting rod and piston) was used to generate the acoustic environment. The slider-crank driving system complicated the flow data by adding undesirable harmonics. As a remedy, a scotch-yoke mechanism was designed and constructed to provide a purer sinusoidal piston motion. The scotch-yoke piston motion provided acoustic flow data that was not complicated by additional harmonics (see Fig. 3 for typical signals derived from either Scotch-yoke or slider-crank wave generators). This facilitated the development and implementation of a meaningful method for performing statistical analysis and reduced the likelihood of noise interference.

Another advantage of the current wave generator is that, when compared with former devices, the larger displacement volume of the Scotch-yoke produces larger acoustic pressure amplitudes. Since the heat of sublimation for dry ice diminishes at higher pressures, increasing the pressure amplitude increases the rate of sublimation. The enhanced pressure-sensivity of dry-ice improves the model's ability to simulate a propellant's pressure response. Unlike Ma's model [12, 13], the enhanced pressure sensitivity obviates the need to use infrared heating lamps to speed up the sublimation process. The absence of an infrared lamp is also beneficial in improving the accuracy of current measurements. Here, they cannot be biased by heat interference with signals gathered from the hot films. In fact, both pressure and velocity data acquired in the experiments are Fourier analyzed to demonstrate the reliability of the driving mechanism.

Two oscillatory flow conditions are investigated in a rectangular chamber purged with CO_2 gas. The two conditions are: (1) oscillatory flow with side-wall injection and (2) oscillatory flow without side-wall injection. It is clear by now that solid CO_2 (dry ice) will be used to simulate side-wall injection. Experiments with side-wall injection are performed for driving frequencies between 2.2 and 50.8 Hz. These result in an acoustic Reynolds number (Re_A) ranging between 80 and 2200. Experiments without side-wall injection are performed for driving frequencies between 2.3 and 44.8 Hz, and $50 < Re_A < 500$. In each of these studies, four types of flow regimes are observed: laminar, distorted laminar, weakly turbulent, and conditionally turbulent.

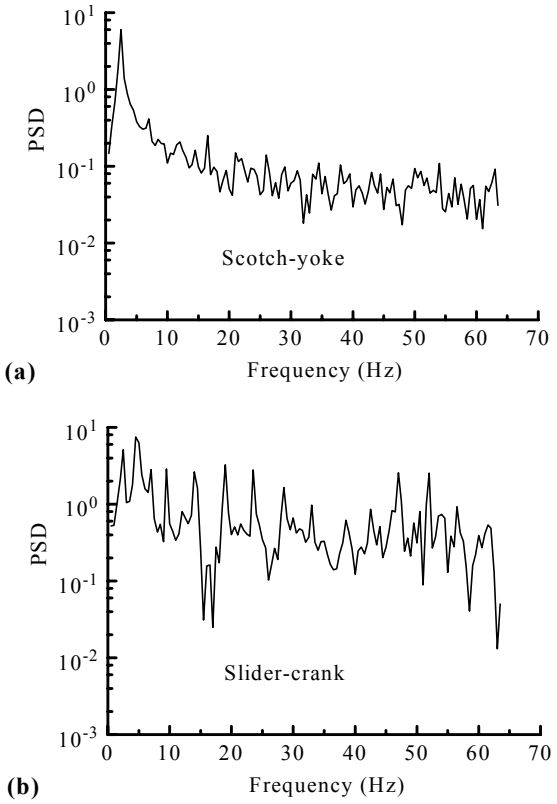

Fig. 3 Power Spectral Density (PSD) of pressure data using (a) Scotch-yoke and (b) slider-crank mechanisms. By comparison, the Scotch yoke provides a purer signal containing less harmonics and noise interference.

4 TRANSITION TO TURBULENCE

Two different methods are implemented to determine the occurrence of turbulence: statistical analysis of acoustic flow data and flow visualization. The statistical analysis of acoustic data provides a systematic method of quantifying the occurrence of turbulence.

In order to perform a statistical analysis of the data, between 10 and 15 data sets are collected at each piston driving frequency. The data sampling frequency is commensurated with frequency of the driving piston. Each data set consists of 512 data points that are collected during a time period of approximately two driving piston cycles. Since the piston frequency ranges between 2.2 and 50.8 Hz, the sampling frequency has been varied between 512 and 10,240 Hz.

Calibration of the hot film anemometer is crucially important. The sensing elements are delicate mechanically and analog output signals have a tendency to drift. Hence, frequent checks of probe calibration are necessary. Hot film anemometers are quite repeatable so accuracy is a function of how closely the calibration conditions are being reproduced in the flow to be measured. For this reason, calibration is performed before each data set is acquired. A flow generator with a plenum chamber and an ASME nozzle are used to get a known air velocity for calibration. The nozzle exit velocity is determined from Bernoulli's equation. An assumption that the static pressure of the air exiting the nozzle is equal to the outside atmospheric pressure is used. A calibration relationship is determined between known velocity and bridge voltage with the hot film probe located at the nozzle exit. The relationship is nonlinear (approximately a ¼ power relation).

4.1 Statistical Analysis

4.1.1 Hard Wall

The maximum standard deviation as a function of acoustic Reynolds number is shown in Fig. 4. For experiments without side-wall injection and $\mathrm{Re}_A < 110$, Fig. 4a indicates that the flow is laminar. The reason is this. An almost linear power law relationship appears to exist between the standard deviation and the Reynolds number. This relationship is of the form $\sigma = a\mathrm{Re}_A^b$, where σ is the standard deviation and a and b are constants. The power law exponent found from least-squares indicates that the standard deviation varies approximately with the square of the acoustic Reynolds number for the laminar case. The standard deviation of the laminar flow is very small (approximately 4% of the maximum velocity amplitude). This is clearly illustrated in Fig. 5 for two typical signals recorded at frequencies of 21 and 36.4 Hz. Distorted laminar flow is observed for $110 < \mathrm{Re}_A < 275$. The largest standard deviations seem to occur in the accelerating and decelerating phases in this regime. The standard deviation for distorted laminar flow is slightly larger than for laminar flow. In fact, a weakly turbulent flow is realized at $\mathrm{Re}_A = 275$. The standard deviations are larger than those for the laminar or distorted laminar cases and the maximum standard deviation occurs at the velocity peaks. A slightly smaller standard deviation is observed in the accelerating phase where turbulence is generated. During the decelerating phase of the same cycle, a sudden drop in standard deviation is noted. This observation indicated that the flow returns to laminar during part of the cycle. The largest standard deviation without side-wall injection occurs in the $\mathrm{Re}_A = 500$ case in which conditionally turbulent flow is achieved. During each cycle, the maximum standard deviation occurs in the decelerating phase where turbulence is generated. In the conditionally turbulent regime, turbulent bursts occur just after the velocity peaks in the decelerating phase. These turbulent bursts are identified by a large standard deviation that appears suddenly, persists for a short time, and then decreases rapidly as the flow returns to laminar. As seen in Fig. 4a, the power law coefficient b relating σ to Re_A drops to near unity in the region corresponding to $\mathrm{Re}_A > 110$. In that range, repeated experiments seem to indicate that the standard deviation becomes of the order of the acoustic Reynolds number as large amplitude turbulence begins to grow.

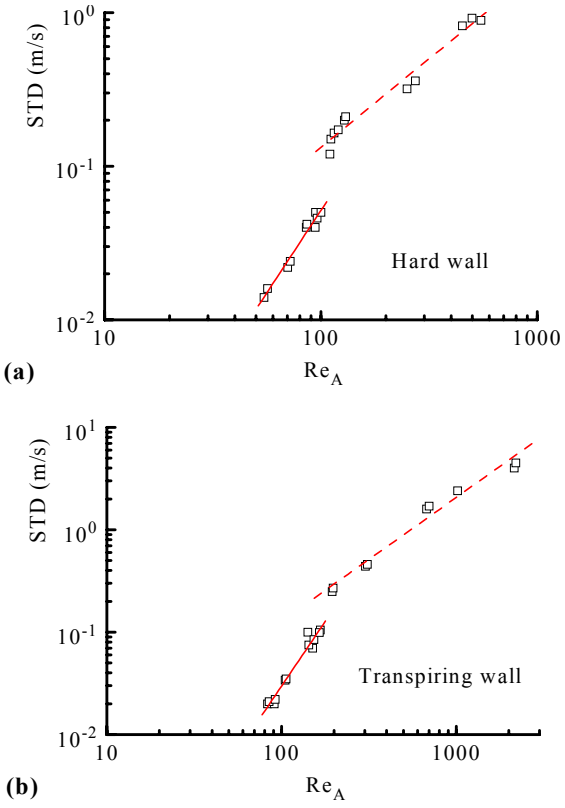

Fig. 4 Standard deviation σ vs. acoustic Reynolds number Re_A for experimental data (□) acquired over (a) hard walls, and (b) transpiring walls using sublimating CO_2. Assuming a logarithmic power law of the form $\sigma \sim \mathrm{Re}_A^b$, linear least-squares indicate the presence of two regions. The first is characterized by $b \cong 2.2$ and is predominantly laminar (——). In the second region, b drops to approximately 1.1, ushering a turbulent flow behavior (- - -).

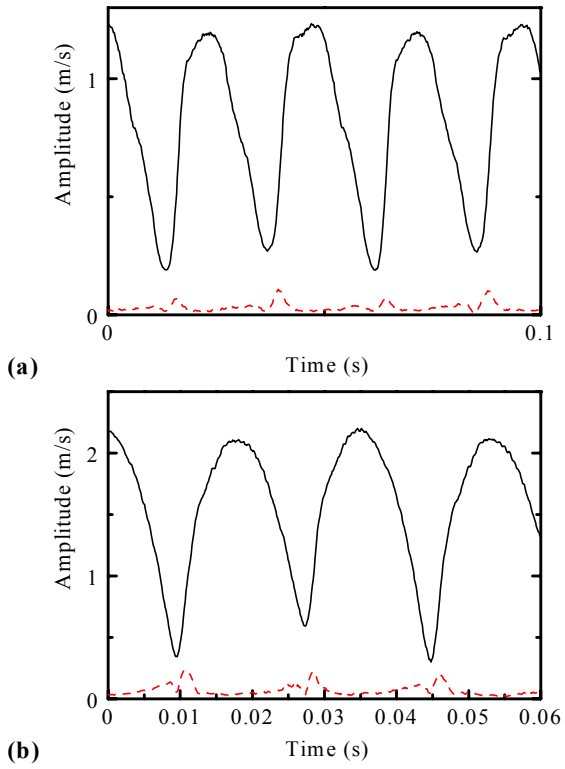

Fig. 5 Using nontranspiring walls, velocity (—) and standard deviations (- - -) are shown for $Re_A = 95$ and 130. The two cases correspond to (a) laminar, and (b) distorted laminar flow regimes.

4.1.2 Transpiring Wall

Maximum standard deviation as a function of the acoustic Reynolds number is shown in Fig. 4b for experiments with side-wall injection. For $Re_A > 140$ the flow is laminar. An almost linear power law relationship also appears to exist between the standard deviation and the acoustic Reynolds number for the side-wall injection case. The power law exponent is approximately 2.2 for the laminar case. The standard deviation of the laminar flow is very small (approximately 4% of the maximum velocity amplitude). Distorted laminar flow is observed for $140 < Re_A < 200$. The largest standard deviations occur in the accelerating and decelerating phases. The standard deviation for distorted laminar flow is slightly larger than for laminar flow. Weakly turbulent flow is observed for $200 < Re_A < 680$. The maximum standard deviation in this regime occurs at the velocity peaks and a slightly smaller standard deviation is observed in the accelerating phase where the turbulence is generated. The standard deviation becomes small during the decelerating phase when relaminarization occurs. Conditionally turbulent flow is observed for $680 < Re_A < 2200$. In this regime, the maximum standard deviation occurs in the decelerating phase where turbulence is generated. In the conditionally turbulent regime, turbulent bursts occur just after the velocity peaks in the decelerating phase. These turbulent bursts are identified by a large standard deviation that appears suddenly, persists for a short time, and then decreases rapidly as the flow returns to laminar. At $Re_A = 2200$, the flow is turbulent during most of the cycle; however, fully turbulent flow was not observed in any of the experiments. In every case, flow was either laminar or relaminarization occurred during some part of the oscillatory cycle. This happened when the periodic amplitude dropped below some threshold value. As seen in Fig. 4b, the power law exponent b relating σ to Re_A decreases to about 1.1 in the region corresponding to $Re_A > 200$. In that region, turbulence begins to dominate during a cycle. Typical signals that illustrate the relative size of the standard deviation in each of the four flow categories are shown in Fig. 6. In addition to being based on relative magnitudes of standard deviations, our flow classification is substantiated by standard flow visualization. This type of qualitative assessment is covered next.

4.2 Flow Visualization

Flow visualization was employed to examine the flow patterns arising in experiments with dry ice in the test section. Under steady state operating conditions, a fog-like layer has been observed above the dry ice. The presence of the fog layer is caused by the water (approximately 1% by weight) that is used to bind the dry ice together during manufacturing. In fact, the behavior of the 'fog' in the flow chamber has been useful both in visualizing the oscillatory Stokes layer, and in qualitatively determining the critical Reynolds number at which transition to turbulence occurs. The flow is considered turbulent when the flow field exhibits high intensity mixing and solid CO_2 particles leave the dry ice surface due to local high intensity instability. Evidently, flow visualization alone is the least conclusive method of detecting turbulence since the analysis is qualitative and the results are somewhat subjective. However, when coupled with statistical measures, it can prove to be quite insightful.

Figure 7 illustrates the general structure of the fog layer during the transitional stages leading to turbulence. The fog layer appears to be uniform across the test section for driving frequencies less than 30 Hz ($Re_A < 200$). The flow also appears to be stable with no indication of mixing (Fig. 7a). This coherent and well-defined structure is taken to be indicative of laminar motion. The smooth lines forming the fog layer can be attributed to the absence of turbulence.

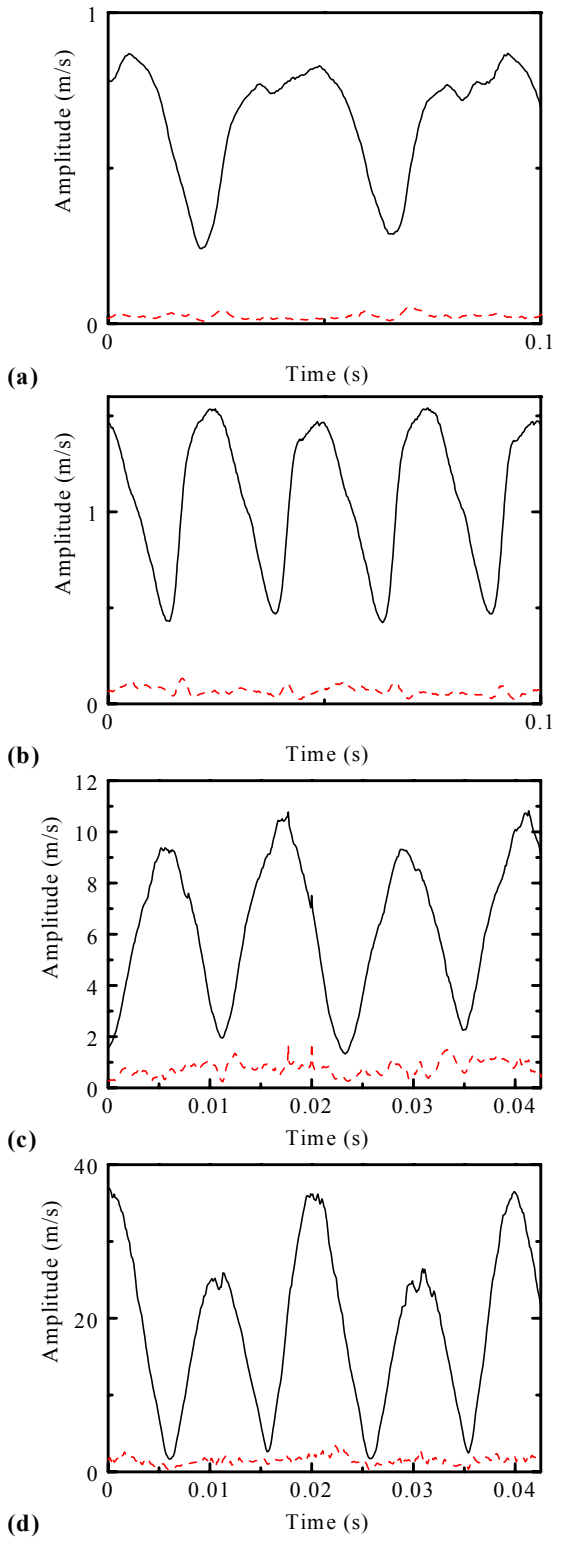

Fig. 6 Using CO_2 wall-injection, velocity (——) and standard deviations (- - -) are shown for $Re_A = 105, 145, 675, 2200$. The cases correspond to (a) laminar, (b) distorted laminar, (c) weakly turbulent, and (d) conditionally turbulent regimes.

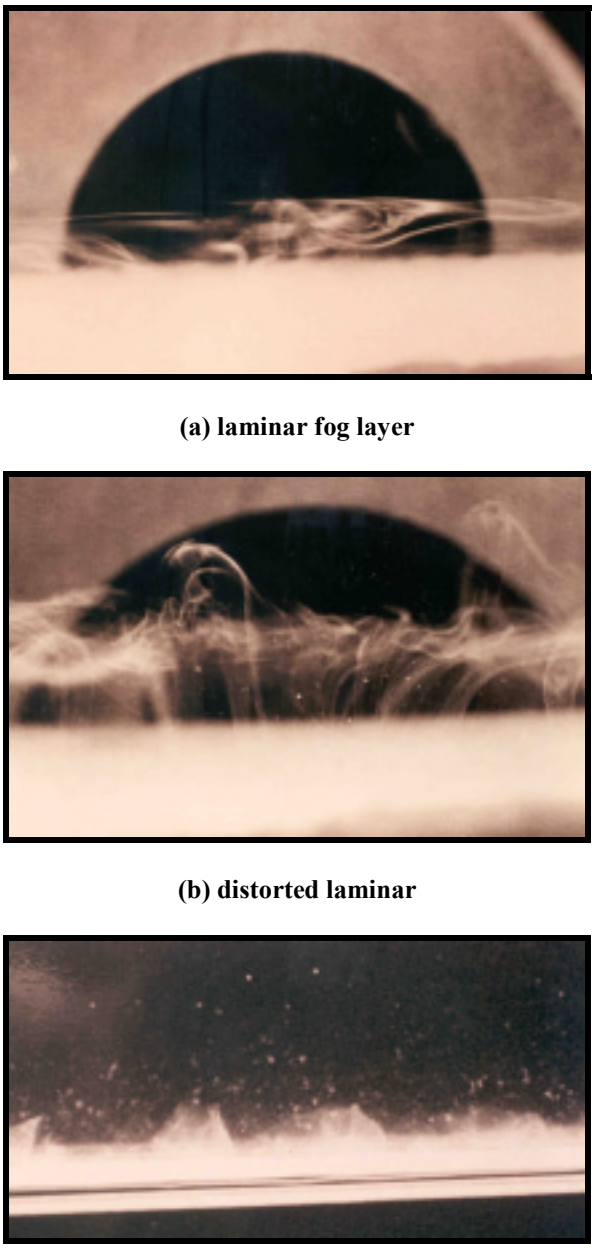

(a) laminar fog layer

(b) distorted laminar

(c) weakly turbulent

Fig. 7 Flow visualization of the oscillatory Stokes layer over a transpiring surface. The close-ups illustrate the detailed structure of the fog layer in (a) laminar, (b) distorted laminar, and (c) weakly turbulent flow regimes.

At approximately 30 Hz ($Re_A = 200$), solid CO_2 particles are observed to leave the dry ice surface due to local high intensity instability (Fig. 7b). For driving frequencies above 30 Hz, the two-dimensional wave propagation is no longer present. The fog layer motion is chaotic and three-dimensional. We conclude that, at driving frequencies greater than 30 Hz, turbulence

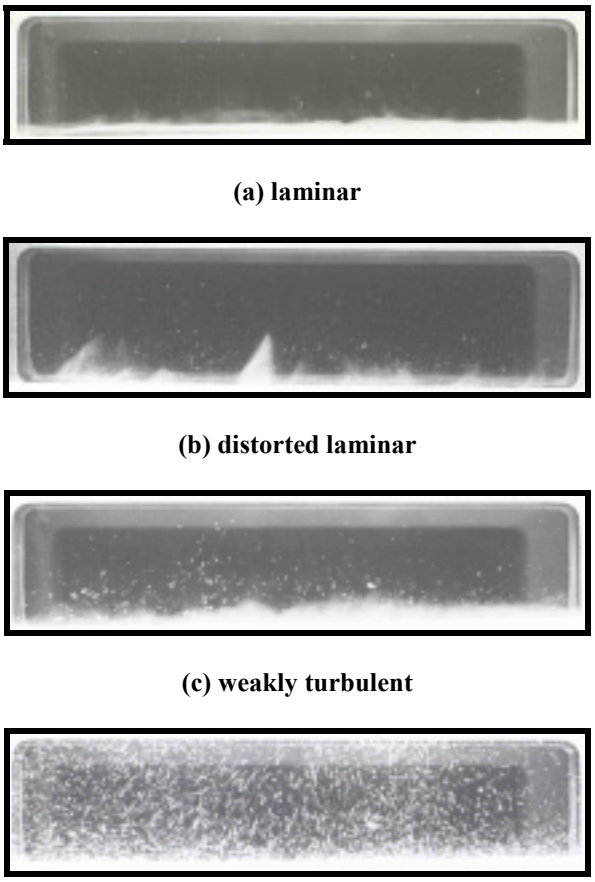

(a) laminar

(b) distorted laminar

(c) weakly turbulent

(d) conditionally turbulent

Fig. 8 Flow visualization of the four distinct phases preceding turbulence. Patterns indicate (a) laminar, (b) distorted laminar, (c) weakly turbulent, and (d) conditionally turbulent flow regimes.

begins to grow. As the driving frequency is varied from 30 Hz to 42 Hz ($200 < \mathrm{Re}_A < 680$), the number of particles ejected from the dry ice surface into the flow field increases and mixing becomes more vigorous as the driving frequency is increased (Fig. 7c). For flow above approximately a 42 Hz driving frequency ($\mathrm{Re}_A = 680$) the fog is no longer visible due to intense mixing. From flow visualization, the critical frequency for transition to turbulence is approximately 30 Hz which is in good agreement with the statistical analysis of the hot film data. In fact, weakly turbulent flow is first seen at 30.4 Hz ($\mathrm{Re}_A = 200$) using statistical analysis. These results are summarized in Fig. 8 where the four distinct patterns of flow are illustrated. Due to the preponderance of physical Reynolds number ranges, Table 1 is provided to summarize our findings.

RANGE Re_A	FLOW REGIME	b	FLOW OBSERVED
OSCILLATORY FLOW OVER TRANSPIRING WALLS			
< 140	Laminar	2.2	A uniform fog layer is visible
140-200	Distorted laminar	1.1	Particles are seen leaving the surface
200-680	Weakly turbulent	1.1	Vigorous mixing & particle ejection
680-2200	Conditionally turbulent	1.1	The fog layer is no longer visible
OSCILLATORY FLOW OVER HARD WALLS			
< 110	Laminar	2.1	Invisible air
110-275	Distorted laminar	1.1	Invisible air
275-390	Weakly turbulent	1.1	Invisible air
390-500	Conditionally turbulent	1.1	Invisible air

Table 1 Summary of experimental observations over different ranges of the acoustic Reynolds number. Results include conclusions from statistical analysis and flow visualization of the Stokes layer over both hard and transpiring walls.

5 SUMMARY

In the current investigation, several experimental deficiencies of previous studies have been addressed. An apparatus that incorporates a nearly pure harmonic wave generator has been successfully constructed and utilized. Substituting the typical slider-crank mechanism by a Scotch yoke led to the remission of undesirable harmonics produced in previous experiments. A data acquisition system controlled by a computer network was capable of collecting many samples of acoustic velocity and pressure data at consecutive cycles and driving frequencies. The method of data collection facilitated statistical analysis of the acoustic data.

The onset of turbulence was investigated for an oscillating flow in a rectangular geometry both with and without side-wall injection. Side-wall injection at the transpiring surface was simulated by the sublimation process of dry ice. This was justified by the fact that sublimating dry ice exhibited many desirable features that we wished to explore. These features include (1) its ability to simulate the burning of a solid rocket propellant; (2) its noninterference with the natural system frequency; (3) its resistance to acoustic dissipation; and (4) its safe handling advantages. Calibrated hot film anemometry was used to record the velocity amplitude near the dry ice surface. Two techniques were used to define the transition from laminar to turbulent regimes: statistical analysis and

flow visualization. Results depended on computer data acquisition and hot film anemometry.

For oscillatory flows over hard walls, Hino [5-8] and coworkers had observed four distinct flow categories in their experiments. These were: (a) laminar, (b) distorted laminar, (c) weakly turbulent, and (d) conditionally turbulent regimes. In order to maintain consistency, continuity, and simplicity, the structures observed in the current experiments were classified in the same four categories. It is hoped that our efforts are shared in helping to standardize the ever-growing nomenclature in periodic flow studies.

The statistical flow analysis showed that the fully turbulent flow regime was not developed even at the highest frequencies permitted by the wave generator. In fact, a relaminarization occurred within every cycle when the velocity amplitude diminished below a certain value. This result is consistent with observations reported in several other studies with nonporous walls. The reader is referred, for instance, to the literature survey of oscillatory flows by Hino and coworkers [5-8].

Through statistical analysis and flow visualization, turbularization of the Stokes layer with side-wall injection was reproducible and repeatable at a critical acoustic Reynolds number of 200. Another important indicator of turbulence was found to be the clear shifting in the power law relationship between the maximum standard deviation and Re_A.

Acknowledgments

The authors wish to thank Dr. David A. Flanigan who has made this project possible through partial funding from the Thiokol Corporation Internal Research and Development. We also wish to thank Professor Richard W. Shorthill from the University of Utah and Dr. Yiping Ma from the Iomega Corporation for helping in the photography and flow visualization. Last, but not least, we wish to thank Mr. Kyle Brucker from Marquette University for helping in the preparation of the final version of the paper.

References

[1] Vincent, G. E., 1957, "Contribution to the Study of Sediment Transport on a Horizontal Bed Due to Wave Action," *Proceedings of the Conference on Coastal Engineering*, 16, pp. 326-335.

[2] Collins, J. I., 1963, "Inception of Turbulence at the Bed under Periodic Gravity Waves," J. Geophys. Res., **68**, pp. 6007-6014.

[3] Sergeev, S. I., 1966, "Fluid Oscillations in Pipes at Moderate Reynolds Numbers," Fluid Dyn., **1**, pp. 21-22.

[4] Merkli, P., and Thomann, H., 1975, "Transition to Turbulence in Oscillating Pipe Flow," J. Fluid Mech., **68**, pp. 567-575.

[5] Hino, M., and Sawamoto, M., 1975, "Linear Stability Analysis of an Oscillatory Flow between Parallel Plates," *Proceedings of the 7th Symposium on Turbulence*, pp. 1-7.

[6] Hino, M., Sawamoto, M., and Takasu, S., 1976, "Experiments on Transition to Turbulence in an Oscillatory Pipe Flow," J. Fluid Mech., **75**, pp. 193-207.

[7] Hino, M., Kashiwayanagi, M., Nakayama, A., and Hara, T., 1983, "Experiments on the Turbulence Statistics and the Structure of a Reciprocating Oscillatory Flow," J. Fluid Mech., **131**, pp. 193-207.

[8] Hino, M., Fukunishi, Y., and Meng, Y., 1990, "Experimental Study of a Three-Dimensional Large-Scale Structure in a Reciprocating Oscillatory Flow," Fluid Dyn. Res., **6**, pp. 261-275.

[9] Ohmi, M., Iguchi, M., Kakehashi, K., and Masuda, T., 1982, "Transition to Turbulence and Velocity Distribution in an Oscillating Pipe Flow," Bull. JSME, **25**, pp. 365-371.

[10] Akhavan-Alizadeh, R., 1987, "An Investigation of Transition and Turbulence in Oscillatory Stokes Layers," Ph.D. Dissertation, MIT.

[11] Traineau, J. C., Hervat, P., and Kuentzmann, P., 1986, "Cold-Flow Simulation of a Two-Dimensional Nozzleless Solid-Rocket Motor," *AIAA*, 86-1447.

[12] Ma, Y., Van Moorhem, W. K., and Shorthill, R. W., 1990, "Innovative Method of Investigating the Role of Turbulence in the Velocity Coupling Phenomenon," ASME J. Vibr. Acoust., **112**, No. 4, pp. 550-555.

[13] Ma, Y., Van Moorhem, W. K., and Shorthill, R. W., 1991, "Experimental Investigation of Velocity Coupling in Combustion Instability," J. Propul. Power, **7**, No. 5, pp. 692-699.

[14] Huesmann, K., and Eckert, E. R. G., 1990, "Studies of the Laminar Flow and the Transition to Turbulence in Porous Tubes with Uniform Injection through the Tube Wall," J. Propul. Power, **6**, No. 6, pp. 690-705.

[15] Dunlap, R., Blackner, A. M., Waugh, R. C., Brown, R. S., and Willoughby, P. G., 1992, "Internal Flow Field Studies in a Simulated Cylindrical Port Rocket Chamber," J. Propul. Power, **8**, No. 6, pp. 1167-1176.